Comparative Evaluation of Bit Error Rate in Frequency Selective Fading Channels Employed in Wavelet Modulation

Sahra S. Jassem

School of Applied Sciences, University of Technology, Baghdad, IRAQ

In this work, results of a comparison modeling treatment of additive white Gaussian noise and two-ray fading channel those affecting the performance of modulation techniques employed in modern communications systems, were presented. The channel parameters were varied to obtain a frequency-selective channel, which was observed by determining the bit error rate as a function of the ratio of signal energy per bit to thermal noise power per Hz. This treatment introduces the performance of wavelet modulation employing such systems.

Keywords: Wavelet modulation, Rayleigh fading channel, Frequency selective channel
Received: 20 April 2008, Revised: 20 May 2008, Accepted: 20 June 2008

1. Introduction

A promising application of wavelet transforms is in the field of digital wireless communications where they can be used to generate waveforms that are suitable for transmission over wireless channels. This type of modulation is known as wavelet modulation (WM) or fractal modulation. The advantage of this scheme emerges from the fact that wavelet modulation allows transmission of the data signal at multiple rates simultaneously.

Wornell and Oppenheim outlined the design of the transmitter and receiver for wavelet modulation (WM) [1]. The performance of wavelet modulation in an additive, white Gaussian noise (AWGN) channel was also evaluated in Ref. [1]. Wornell showed that the bit error rate (BER) performance of wavelet modulation is a function of signal-to-noise ratio (SNR) in the channel; the estimate of the received bit becomes more accurate as the number of noisy observations used to calculate it is increased. Ptasinski and Fellman simulated wavelet modulation using the Daubechies N=4 wavelet and measured its BER performance in an AWGN channel [2]. The performance of wavelet modulation was shown to be equivalent to that calculated by Ref. [1] (i.e. the results were equivalent to binary phase shift keying (BPSK) performance for the AWGN channel) [2]. In all of the previous research, the BER performance was measured using a single scale (i.e. rate) for demodulation.

Wavelets have also been proposed for use in other aspects of communication systems. Multiple access schemes using orthogonal wavelet-based codes have been proposed as an alternative to code division multiple access (CDMA) [3,4]. Wavelet-based modulation techniques for frequency-hopped spread spectrum communications have also appeared in the literature [5,6] as the wavelet packet transform. An extension of the wavelet transform, in which the high pass branches are iterated as well as the low pass branches, has led to the development of wavelet packet modulation (WPM). This modulation technique exploits the larger selection of time-frequency tailings at its disposal to minimize channel disturbances [7,8].

A fading channel is modeled with a multiplicative fading component and an additive noise component. The order of simulation complexity for such a process for 1-D modulations is one addition and one multiplication. For 2-D modulation methods, the complexity for one symbol is one complex multiplication and one complex addition per symbol. This is equivalent to four real multiplications and four real additions for each symbol [9].

2. Modeling Procedure

Clarke [5] has proposed a statistical model for the received signal amplitude of the flat-fading channel based on scattering propagation. Gans [10] has further shown that in the case of isotropic, two-dimensional scattering with an omni-directional receiving antenna, the quadrature Gaussian processes representing the fading have autocorrelation function (ACF) [11].

The most common channel model encountered in communications systems is the additive white Gaussian noise (AWGN) channel. In this channel, zero-mean white Gaussian noise is added to the transmitted signal $s(t)$, so that the received signal $r(t)$ can be represented as:

$$r(t) = s(t) + n(t) \quad (1)$$

where $n(t)$ is a zero-mean white Gaussian noise process. $N_o/2$ is the power spectral density of the noise term $n(t)$.

The time dispersion in a multi-path environment causes the signal to undergo either flat or frequency selective fading. If the channel has a constant gain and linear phase response over a bandwidth that is greater than the bandwidth of the transmitted signal, then the received signal undergoes flat fading (i.e. the received signal is not distorted by inter-symbol interference). In a flat fading, channel the signal bandwidth is much smaller than the coherence bandwidth of the channel. Alternatively, time dispersion can be described in terms of the symbol period (T_S). In a flat fading, channel T_S is much larger than the root-mean-square (r.m.s) delay spread of the channel (σ_τ). In these wavelet modulation trials T_S at scale 10 is 0.977ms and T_S at scale 13 is 122µs. The form of this simulated model, Eq. (2), results in a flat fading channel for all scales (i.e. $\sigma_\tau << T_{S13} < T_{S10}$) since σ_τ is effectively zero in this model.

Small scale fading can be modeled as a Rayleigh distribution [12,13]. The received signal is given by

$$r(t) = s(t)R(t) + n(t) \quad (2)$$

As in the AWGN channel, $s(t)$ is the transmitted signal and $n(t)$ represents thermal and device noise (it also still dictates the SNR). The impact of the Rayleigh, flat, slow fading channel is given by the multiplicative $R(t)$ [12]. The function $r(t)$ is coherently demodulated; perfect carrier synchronization is assumed at the receiver.

If the bandwidth of the signal of interest exceeds the coherence bandwidth of the channel, the signal undergoes frequency selective fading. In the frequency domain, the channel causes different levels of attenuation for different frequency components of the signal. Frequency selective fading is caused by multi-path delays which approach or exceed the symbol period of the transmitted symbol (i.e. $T_S < \sigma_\tau$), where σ_τ is still the r.m.s delay spread of the channel. In practice, $T_S \leq 10\sigma_\tau$ will result in a frequency selective channel as the channel introduces ISI.

I have used a two-ray channel model with a variable r.m.s delay spread σ_τ. (σ_τ was varied between 0.2µs and 120µs). In propagation measurements by Reference [14] at 900MHz, urban areas typically had r.m.s delays in the range of 2−3µs, hilly residential areas had r.m.s delays in the range of 5−7µs and worst case r.m.s delay spreads were of the order of 20µs. Excess delays in the range of 100µs were also observed. For the frequency selective fading channel, the received signal is given by:

$$r(t) = \alpha_0 R_0(t)s(t) + \alpha_1 R_1(t)s(t-\tau_1) + n(t) \quad (3)$$

where α_0 and α_1 are the amplitudes of the main ray and the secondary ray, respectively.

The signal energy in the main component along with the power of the noise term, $n(t)$, determines the SNR of the signal. The secondary component with a factor of α_1 and delayed by τ_1 corresponds to the first multi-path bin with significant amplitude.

The r.m.s delay spread is defined as [12]:

$$\sigma_\tau = \sqrt{\overline{\tau^2} - (\overline{\tau})^2} \quad (4)$$

where τ is the mean excess delay and is defined by:

$$\overline{\tau} = \frac{\sum_k P(\tau_k)\tau_k}{\sum_k P(\tau_k)} \quad (5)$$

where $P(\tau_k)$ is the power of the k^{th} component (ray) and is obtained from the power delay profile of the channel and τ_k is the delay of the k^{th} component. All delays are measured relative to the first signal arriving at τ_0=0. The second moment of the power delay profile (τ_2) is given by:

$$\overline{\tau^2} = \frac{\sum_k P(\tau_k)\tau_k^2}{\sum_k P(\tau_k)} \quad (6)$$

For these experiments, I simulate two paths so that k=0 and k=1. Furthermore, in many of these trials, $\alpha_0 = \alpha_1$; thus Eq. (4) simplifies to $\sigma_\tau = \tau_2$. Now, $P(\tau_k)$ is given by α_{2k} where α_k is the amplitude (gain) of the k^{th} ray.

The sum of $E\{\alpha^2_0 R_0(t)^2\}$ and $E\{\alpha^2_1 R_1(t)^2\}$ is set to unity so that the channel has an average power gain of one [15]. This is to ensure that the average signal energy at the input and output of the channel remains the same. A generalized block diagram of a frequency selective channel is shown in Fig. (1) for an N-path channel. For frequency-selective channel in (3), N=2 [12].

In Fig. (1), the Rayleigh waveform $R_{N-1}(t)$ can be generated using Clarke [5] and Gans [10] fading model. A Rayleigh fading waveform can be simulated by generating independent in-phase and quadrature complex Gaussian noise samples and filtering them by $H(f)$ as shown in Fig. (2). $S_{Ez}(f)$ is the spectrum of the Doppler filter. Particularly, it has been shown that for an omni-directional λ/4 antenna with a gain of 1.5, the Doppler spectrum is given by [16]:

$$S_{E_z}(f) = \frac{1.5}{\pi f_m \sqrt{1 - (\frac{f - f_c}{f_m})^2}} \quad (7)$$

where f_c is the center frequency and f_m is the maximum Doppler spread. The frequency f_c is

zero and f_m takes values of 60Hz and 120Hz. The sum of the in-phase and quadrature terms at the output of the inverse fast Fourier transformation (IFFT) forms the complex Rayleigh fading waveform $R_{N-1}(t)$. The waveform has a Rayleigh distributed amplitude and a uniformly distributed phase in the interval [0,2π). The r.m.s value of the envelope is normalized to one. This normalization ensures that the average signal energy is not altered when passed through the channel simulator. This complex, normalized waveform is denoted as $R_{N-1}(t)$ in Fig. (2). These Rayleigh waveform generators are used to generate each of the $R_k(t)$ in Fig. (1) where k is from 0 to N-1. The waveform $R(t)$ in Eq. (2) is obtained by taking only the envelope component (i.e. $R(t)=|R_{N-1}(t)|$) of the complex fading waveform generated in Fig. (2).

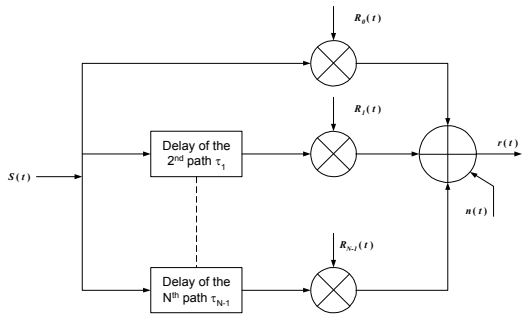

Fig. (1) Frequency-selective channel model

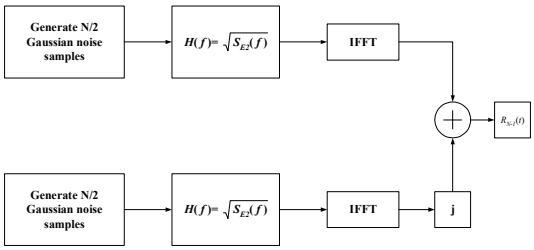

Fig. (2) Generation of a Rayleigh fading waveform

The wavelet representation of a signal $s(t)$ is given by [16]:

$$s_n^m = \int_{-\infty}^{\infty} s(t) 2^{m/2} \psi(2^m t - n) dt \qquad (8a)$$

$$s(t) = \sum_{m=-\infty}^{\infty} \sum_{n=-\infty}^{\infty} s_n^m 2^{m/2} \psi(2^m t - n) \qquad (8b)$$

where $\psi(t)$ is the wavelet function [17].

The resolution limited approximation of a signal $s(t)$ is given by

$$A_{m+1} s(t) = \sum_n a_n^{m+1} \phi_n^{m+1}(t) \qquad (9)$$

where the function a_n^{m+1} produces the approximation coefficients obtained by the projection of $s(t)$ onto the basis functions:

$$a_n^{m+1} = \int_{-\infty}^{\infty} s(t) \phi_n^{m+1}(t) dt \qquad (10)$$

The approximation and wavelet coefficients can be calculated at any scale by:

$$a_n^m = \sum_l h(1-2n) a_l^{m+1} \qquad (11a)$$

$$s_n^m = \sum_l g(1-2n) a_l^{m+1} \qquad (11b)$$

where $h(-n)$ and $g(-n)$ are the low-pass and high-pass filters in the associated 2 channel analysis filter bank. Eq.s (10a) and (10b) represent the fast wavelet transform (FWT) needed to compute the discrete wavelet transform (DWT) in Eq. (8) and Fig. (3) shows the analysis filter bank corresponding to the DWT.

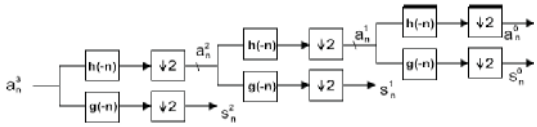

Fig. (3) A two-channel analysis filter bank used to compute the DWT

Conversely, it is possible to reconstruct the approximation coefficients a_n^m using the following equation:

$$a_n^{m+1} = \sum_l h(2l-n) a_l^m + g(2l-n) s_l^m \qquad (12)$$

The reconstruction process is shown in Fig. (4). This is the inverse FWT (IFWT) needed for computing the inverse DWT (IDWT) in Eq. (8b). In Fig. (4), $h(n)$ and $g(n)$ are the low-pass and high-pass synthesis filters. The low-pass filter ($h(n)$) satisfies the following orthogonality condition:

$$\sum_n h(n) h(n-2k) = \delta(k) \qquad (13)$$

The highpass filter is obtained from the low-pass filter by:

$$g(n) = (-1)^n h(N-n) \qquad (14)$$

where $(N+1)$ is the filter length.

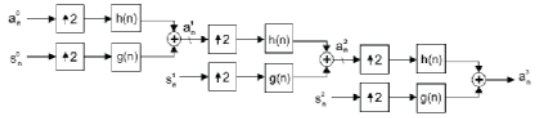

Fig. (4) A two-channel synthesis Filter bank to compute the IDWT

Together, Eq.s (11a), (11b) and (12) form the DWT and the IDWT. These discrete time algorithms with filter bank implementations are used in wavelet modulation.

The wavelet modulated signal to be transmitted, $s(t)$, can be generated by:

$$s(t) = a^{-H} y(at) \qquad (15)$$

where $x[n]$ is the data that is modulated onto the wavelet at different scales $\beta=2^{2H+1}$ where H refers to the degree of the homogeneous signal. A homogeneous signal $y(t)$ satisfies the self-invariance property:

$$y(t) = a^{-H} y(at) \tag{16}$$

where $a>0$ [1]. I take $H=-1/2$ so that $\beta=1$. Note that $s(t)$ is completely specified by $x[n]$. Contrarily, $x[n]$ is referred to as the generating sequence for the transmitted signal $s(t)$.

In a practical system, $x[n]$ is modulated onto a finite number of contiguous, octave-width frequency bands (i.e. m has finite limits and there are a finite number of scales available). Consequently, the transmitted signal $s(t)$ is given by [17]:

$$s(t) = \sum_{n=-\infty}^{\infty} \sum_{m \in M} \beta^{-m/2} x[n] 2^{m/2} \psi(2^m t - n) \tag{17}$$

where M is a finite set of contiguous integers.

For the data to be recovered at rate 2^m, the smallest baseband bandwidth that can be used is 2^{m+1}Hz. This results in a bandwidth efficiency of η_F=0.5bits/sec/Hz, which represents a disadvantage of wavelet modulation when compared to traditional modulation techniques like differential quadrature phase shift keying (QPSK) or 16-QAM with bandwidth efficiencies of η_F=2.0bits/sec/Hz and η_F=4.0bits/sec/Hz, respectively.

However, wavelet modulation has an advantage over traditional modulation techniques in its novel multirate diversity. For instance, in wavelet modulation, if some frequency bands are corrupted, then the message can still reach the receiver on one of the uncorrupted frequency bands (i.e. scales). Hence, wavelet modulation works well in fading environments where other modulation techniques suffer poor performance. In other words, only one copy of the message needs to get through.

These simulations have been carried out for two different sets of scales. Therefore, the scale parameter m takes on two sets of values as follows:

1. $m \in M$ where M={10, 11, 12, 13}; this corresponds to a data rate of R_b=1024bps for binary data at the coarse scale (m=10) and R_b=8192bps at the fine scale (m=13). For demodulation at the receiver, a baseband bandwidth of 2^{m+1}Hz is required [1]. Consequently, demodulation at scale m=13 requires a bandwidth of 2^{13+1}=16 kHz.

2. $m \in M$ where M={14, 15, 16, 17}; this corresponds to a data rate of R_b=16.384kbps for binary data at the coarse scale (m=14) and R_b=131kbps at the fine scale (m=17).

The data to be transmitted takes on one of two equally probable values:

$$x[n] \in \{+\sqrt{E_b}, -\sqrt{E_b}\} \tag{18}$$

where E_b is the energy per bit.

By comparing Eq.s (8b) and (15) and remembering that β=1, I note that the wavelet coefficients of $s(t)$ correspond to the data $x[n]$. Thus, $x[n]$ is used instead of s_l^m in Eq. (12) to obtain the approximation of $s(t)$ at scale m+1. Note that to compute the transmitted signal $s(t)$ I use the IFWT (Eq. 12) instead of Eq. (17), where a_n^{m+1} is the approximation of $s(t)$ at scale m+1.

The data to be transmitted ($x[n]$) is split into blocks of length L=1024. To begin the generation of $s(t)$, I begin at the coarse scale m=10; the data is convolved with the filter coefficients of the highpass filter, $g(n)$. Eq. (12) is simplified to:

$$a_n^{11} = \sum_l g(2l-n) x_l^{10} \tag{19}$$

where x_l^{10}, the data to be transmitted at scale 10, is given by the vector:

$x_l^{10} = x = [x[0], x[1], \ldots x[1023]]$

Twice the amount of data is required to modulate the data onto the next higher scale. A periodic replication of the data results in:

$x_l^{11} = [x\ x] = [x[0], x[1], \ldots x[1023], x[0], x[1], \ldots x[1023]]$

Then a_n^{12} (the approximation of $s(t)$ at scale 12) is obtained by Eq. 12 as:

$$a_n^{12} = \sum_l h(2l-n) a_l^{11} + g(2l-n) x_l^{11} \tag{20}$$

A view of the transmitted signal in the time-frequency plane is shown in Fig. (5). At scale 11 there is twice the amount of data at scale 10. Eq. (20) is repeated until the coefficients at scale 14, a_n^{14}, are obtained. These coefficients are iterated through the filter bank again with x_l^m=0 until approximation coefficients at scale 17 (a_n^{17}) are obtained. This results in a close approximation to the signal $s(t)$ with a sampling rate of 131072 samples/sec and this signal is then transmitted over the channel to the receiver.

Fig. (6) presents a block diagram for the implementation of the wavelet modulation simulator. The IDWT (implemented using the IFWT) performs the function of the transmitter and the DWT (implemented using the FWT) performs the function of the receiver. The decision device estimates the transmitted bit from the received data. If the received data is greater than zero, then the transmitted bit is $+\sqrt{E_b}$; if not, then the transmitted bit is $-\sqrt{E_b}$. The data comparator/verification step compares the received data with the transmitted data and determines the error rate. An error occurs if the received bit does not match the transmitted bit. In practice, the output signal $s(t)$ would be multiplied by a carrier at some pass-band frequency (ω_c) to obtain the band-pass signal.

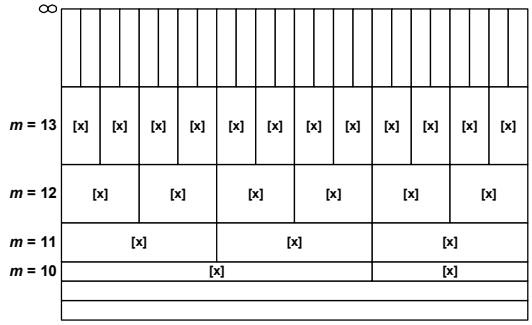

Fig. (5) Time-frequency portrait of the transmitted signal *s*(*t*). [*x*] represents data blocks of length *L*=1024 bits

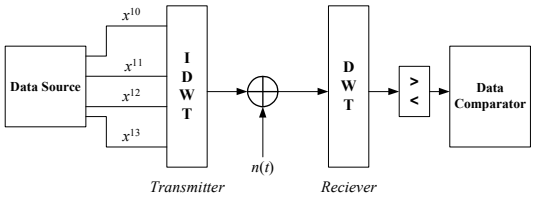

Fig. (6) Block diagram of WM simulator with an additive white Gaussian noise channel

The scaling constants α_0 and α_1 in Eq. (3) were 0.707 and 0.707, respectively, to give a main (carrier) ray to secondary (delayed) ray power ratio of 0dB, i.e.

$$E\{\alpha_0^2 R_0(t)^2\}E\{\alpha_1^2 R_1(t)^2\}=1 \quad (21a)$$

or

$$C/D = 0 \text{ dB} \quad (21b)$$

where C is the power in the main ray and D is the power in the delayed ray). The channel coefficients are normalized such that the average signal energy at the input to the channel is the same as the energy at the output. Recall that τ in Eq. (3) is $0.5T_{Si}$, where $12 \le i \le 17$ (T_{Si} refers to the bit period at scale i) and τ and σ_τ are related by $\sigma_\tau=\tau^2$. The r.m.s delay spread was varied from 1.9μs ($\tau=0.5T_{S17}$) to 61μs ($\tau=0.5T_{S12}$). Coherent demodulation was performed at the receiver for all transmitted scales.

For Gaussian distributed noise, the error probability can be calculated using the Q function defined by [18]:

$$Q(x)=\frac{1}{\sqrt{2\pi}}\int_x^\infty \exp\left(\frac{-t^2}{2}\right)dt \quad (22)$$

The function $Q(x)$ represents cumulative values of the Gaussian distribution.

The SNR of the channel at the receiver is usually the factor that determines the ease with which signal can e recovered. However, for a digital signal, it is the energy per bit and how much bandwidth is used, rather than the average signal and noise powers, that are the critical factors in determining how much of a problem the noise might cause. Hence, the ratio of signal-power-to-noise-power is better described by the ratio of signal energy per bit to thermal noise power per Hz (E_b/N_0) where $E_b=\boldsymbol{S/K}$ is the ratio of the signal power $\boldsymbol{S}$ to the data rate $\boldsymbol{K}$ (not the signal element rate), $N_0=\boldsymbol{N/B}$ is the noise power per Hz, where $\boldsymbol{N}$ is the total noise power and $\boldsymbol{B}$ is the bandwidth of the channel. Hence, E_b/N_0 is a measure of the worth of a channel used for digital signals, just as SNR is a measure of the worth of a channel used for analog signals.

For unipolar signaling, the bit error rate (BER) and E_b/N_0 are related by [18]:

$$BER = Q\left(\sqrt{a\frac{E_b}{N_0}}\right) \quad (23)$$

where a is a constant determined by the line coding scheme.

3. Results and Discussion

The inter-symbol interference (ISI) adversely impacts scales 16 and 17, but affects scale 14 to a comparatively lesser degree. Scales 14 and 15 show better performance than BPSK. This unique characteristic of wavelet modulation can be exploited to obtain better BER performance in mobile environments. For instance, if the worst case delay spread ($\sigma_{\tau max}$) of a particular environment were known, then the demodulation would be performed at the scales where the channel is flattest (i.e. scales where $T_{Si} \ge 10\sigma_{\tau max}$).

Now consider four different scales; scales 10 through 13 are transmitted over the frequency-selective channel. The r.m.s delay spread is 15.3μs which is $0.125T_{S13}$ ($\tau=0.25T_{S13}$). Fig. (7) depicts the BER performance. Scales 10 and 11 show error floors lower than 10^{-2}. Scales 12 and 13 display poorer BER performance since the ISI is larger at those scales.

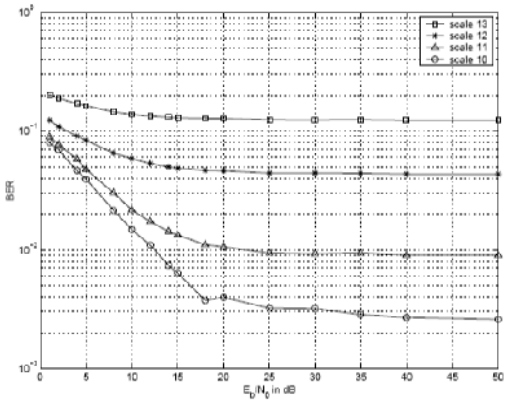

Fig. (7) Bit Error Rate (BER) vs. E_b/N_0 in a frequency selective, slow fading channel with f_d=60Hz and σ_τ=15.3μs=0.125T_{S13} (τ=30.5μs=0.25T_{S13})

Further simulations were performed for larger r.m.s delay spreads. Fig. (8) shows the BER performance for all scales when the r.m.s delay spread is $0.25T_{S12}$ ($\tau=0.5T_{S12}$). In Fig. (8), scales 11, 12 and 13 perform poorly while scale 10 shows a slightly better performance.

Furthermore, scale 13 has a lower error floor than scale 12.

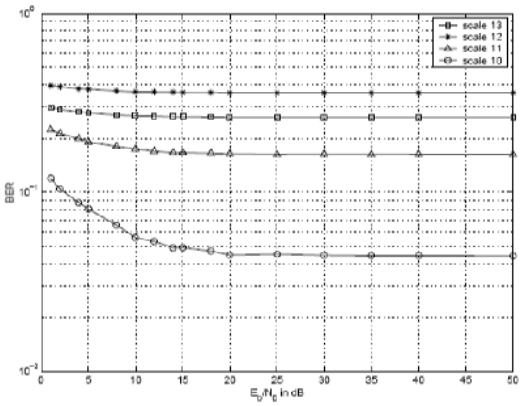

Fig. (8) Bit Error Rate (BER) vs. E_b/N_0 in a frequency selective, slow fading channel with f_d=60Hz and σ_τ=61μs =0.25T_{S12} (τ=0.5T_{S12})

When comparing both figures to each other, a gradual degradation of performance is seen for scale 10 demodulation as the delay τ is increased; scale 10 shows the best performance in Fig. (7) (i.e. for σ_τ=0.125T_{S13}) and the worst performance in Fig. (8) (i.e. for σ_τ=0.25T_{S12}). This is due to the increase in ISI for scale 10 data as the delay between the paths is gradually increased. At σ_τ=0.25T_{S12} (Fig. (8)), the second ray is delayed by half a symbol at scale 12 resulting in the distortion of the received signal at that scale and at scale 10 (due to ISI) from which the receiver cannot recover.

Furthermore, assuming a minimum BER of 10^{-2}, it is observed that the number of scales that can be used for demodulation decreases as the value of τ is increased. In particular, for τ=0.25T_{S13} (Fig. (7)), scales 10 and 11 can be used for demodulation. Hence, an intelligent selection of demodulation scales at the receiver can result in superior BER performance.

4. Conclusions

When the delay spread of a particular environment is known, the demodulation would be performed at the scales where the channel is flattest. It was observed that the number of scales that can be used for demodulation decreases as the value of the mean excess delay is increased. Since the results for the 120Hz channel do not vary appreciably from that which was observed for the 60Hz channel, it can be concluded that the limit on the BER is due to the ISI in a frequency-selective channel.

References

[1] G. Wornell and A. Oppenheim, *IEEE Trans. Information Theory*, 38 (1992) pp.785-800.

[2] H.S. Ptasinski and R.D. Fellman, "Implementation and simulation of a fractal modulation communication system", *Proc. IEEE SUPERCOMM/International Communications Conference*, 3 (1994) pp.1551-1555.

[3] D. Cochran and C. Wei, "A wavelet-based multiple-access spread spectrum modulation scheme", *13th Annual IEEE International Conference on Computers and Communications*, (1994), pp.461-464.

[4] E.J. Yi and E.J. Powers, "Wavelet-based orthogonal modulation code", *Proc. 33rd Asilomar Conference on Signals, Systems and Computers*, (1999) pp.674-692.

[5] R.H. Clarke, *Bell Systems Technical Journal*, 47 (1968) pp.957-1000.

[6] J.G. Proakis, S. Srinidhi and M. Stojanovic, "Wavelet based modulation for frequency hopped spread spectrum communications", *49th IEEE Vehicular Technology Conference*, 2 (1999) pp.904-908.

[7] H.M. Newlin, "Developments in the use of wavelets in communication systems", *Proceedings of MILCOM*, (1998) pp.343.349.

[8] G. Bi, W. Yang and T.P. Yum, "A multirate wireless transmission system using wavelet packet modulation", *47th IEEE Vehicular Technology Conference*, (1997) pp.368-372.

[9] G. Karabulut and A. Yongacoglu, "Additive model for Rayleigh fading channel", *Online article* (2005).

[10] M.J. Gans, *IEEE Trans. Vehicular Technol.*, VT-21 (1972) pp.27-38.

[11] C.C. Tan and N.C. Beaulieu, *IEEE Trans. Commun.*, 48(12) (2000), pp.2032-2040.

[12] T. Rappaport, "**Wireless Communications**", Prentice Hall (NJ), 1st edition, 1996.

[13] B. Sklar, *IEEE Communications Magazine*, 35(7) (1997) pp.90-100.

[14] S. Siedel, T. Rappaport and R. Singh, *IEEE Trans. Vehicular Technol.*, 39(2) (1990) pp.132-139.

[15] T. Rappaport, V. Fung and B. Thoma, *IEEE Trans. Inform. Theory*, 11(3) (1993) pp.393-405.

[16] I. Daubechies, **"Ten Lectures on Wavelets"**, SIAM (Philadelphia, PA), 1st edition, 1992.

[17] M.J. Usher and C.G. Guy, **"Information and Communication for Engineers"**, Macmillan Press, Ltd. (Hong Kong) (1997), pp.158-161.

[18] M. Wu, Y.H. Chew and T.T. Tjhung, *Int. J. Wireless Opt. Commun.*, 1 (2003) pp.41-52.

